A wind turbine two level back-to-back converter power loss study

Ivan Mrčela
University of Zagreb
Faculty of Electrical
Engineering and Computing,
Croatia,
Email: ivan.mrcela@fer.hr

Damir Sumina
University of Zagreb
Faculty of Electrical
Engineering and Computing,
Croatia,
Email: damir.sumina@fer.hr

Filip Sačić
University of Zagreb
Faculty of Electrical
Engineering and Computing,
Croatia,
Email: filip.sacic@fer.hr

Tin Bariša
University of Zagreb
Faculty of Electrical
Engineering and Computing,
Croatia,
Email: tin.barisa@fer.hr

***Abstract*—Wind power conversion systems are a widespread renewable energy source and, as such, have been studied intensely over the past two decades. Wind energy conversion system is connected to the electrical grid through a power converter, an *LC* filter and a step-up transformer. It is necessary to know the efficiency of the whole energy transfer system and to know the efficiencies of each individual part of that system, i.e. converter, filter and transformer efficiencies, in order to achieve a high-efficiency energy conversion system. This paper presents a simulation model used to determine the grid- and generator-side inverter losses, *LC* filter and step-up losses, total converter losses and converter efficiency, as well as grid voltage THD and grid and converter current THDs. This paper also decribes the method used to determine the maximum torque per amp (MTPA) algorithm parameters, used to control the generator-side inverter. Simulations were done at nominal operating conditions, as well as for varied DC link and grid voltages, ranging from zero to nominal converter power.**

***Index Terms*—Back-to-back converter, internal permanent magnet syncronous generator, converter losses, converter efficiency, MTPA**

I. Introduction

Share of renewable energy sources in overall energy production has been continuously growing for the past two decades, [1]. In general, electric power is generated from wind using an electric generator and a power converter. A permanent magnet generator with a full-scale back-to-back converter is one of the more attractive solutions. The power converter's efficiency affects the overall wind energy conversion systems (WECS) efficiency and depends on the power modules used, switching frequency, operating point, selected modulation and working temperature. The DC link is connected to the electric grid via an inverter, a grid-side output filter and a step-up transformer. The inverter is used for DC/AC voltage conversion with a predefined fundamental harmonic frequency and amplitude, via pulse-width modulation (PWM). Fig. 1 shows a basic electrical schematic of the analyzed back-to-back converter, together with its electrical source (wind turbine and PMG) and load (*LC* filter, step-up transformer and the electrical grid).

The proposed paper's objective is to investigate switching loss for a full scale two level back-to-back converter used in WECS, to determine the grid-side inverter loss, the generator-side inverter loss, the *LC* filter and the DC link loss, as well as the output voltage and current THD, all depending on generator true power variations, from generator idle to nominal generator active power, in order to determine the maximum energy conversion efficiency point. The goal is also to analyze the grid voltage and DC link voltage fluctuations influence on the converter power loss and on the grid-side voltages and currents. This paper addresses the aforementioned problems and focuses on analyzing and simulating the effects grid and DC link voltage fluctuations have on power converter losses. The presented analysis and simulation results represent this paper's contribution.

A laboratory model-based simulation model of a permanent magnet generator (PMG) and a 520 kW back-to-back converter was developed in PLECS in order to simulate the back-to-back converter power loss. Control structures of grid-side and generator-side inverters were developed and the controller's parameters were adjusted using magnitude and symmetric optimums.

An instantaneous switching and conduction losses simulation block was developed as part of a larger simulation model. Switching loss is approximated from semiconductor datasheets using a third-order polynomial of the instantaneous switching energy as a switching current variable. The power loss block contains additional switching detection and current direction blocks for each semiconductor switch in order to determine the instantaneous switching energy, used to determine the converter switching loss. Two modulations were selected: space vector PWM (SVPWM) with maximum torque per amp (MTPA) algorithm on the generator-side, and third harmonic injection PWM (THIPWM) on the grid-side. There are several ways to expand the sine modulation linear range, and THIPWM was chosen for it's simple implementation and good overall results.

Since the output filter and step-up transformer are an integral part of most converters connected to a wind turbine generator, their losses were simulated in an effort to determine overall efficiency of the system.

978-1-5090-1797-3/16/$31.00 ©2016 IEEE

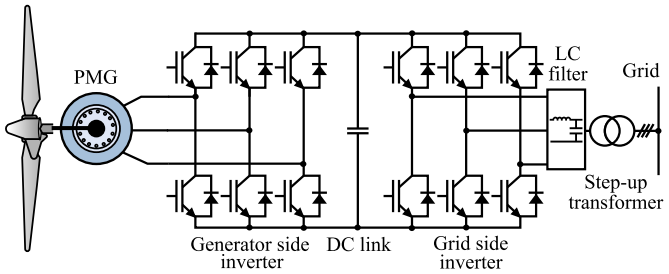

Fig. 1. Wind energy conversion system

TABLE I
PMG PARAMETERS

Nominal power P_{n}	$375\,\mathrm{kW}/1500\,\mathrm{min}^{-1}$ $450\,\mathrm{kW}/1800\,\mathrm{min}^{-1}$
Back EMF constant	$266\,\mathrm{V/kmin}^{-1}$
Nominal current I_{n}	596 A
Nominal torque $T_{\mathrm{em,\,n}}$	2389 N m
Stator resistance R_{s}	$8,05\,\mathrm{m\Omega}$
d-axis inductance L_d	$0,72\,\mathrm{mH}$
q-axis inductance L_q	$1,06\,\mathrm{mH}$
Permanent magnet flux linkage Ψ_{f}	$0,69\,\mathrm{Wb}$

II. A TWO LEVEL BACK-TO-BACK CONVERTER SIMULATION MODEL

Fig. 2 shows the converter simulation model. The model consists of two three-phase two-level inverters (generator and grid-side), a DC link with a braking chopper between them, three AC voltage sources modelling the electrical grid, a three-phase generator model, an *LC* filter, a step-up transformer and control structures for each side of the converter (generator and grid). A braking chopper is cruicial in grid fault situations, in order to keep the DC link voltage value within set values. If a grid fault situation occurs during steady-state operation, DC link voltage rises and is instantly limited by the brake chopper.

PMG model parameters are shown in Table I. Converter model parameters are shown in Table II. Parameter values in Table I and Table II are based on parameter values of a full-scale laboratory model.

A. Grid-side inverter control

Fig. 3 shows the grid-side inverter control scheme [2]. Grid-side inverter consists of three phases, each consisting of two IGBT-freewheeling diode modules. An IGBT with a freewheeling diode is a bidirectional semiconductor switch, allowing a bidirectional energy flow.

The control circuit consists of two control loops. The outer loop controls the DC link voltage using a PI controller. Outer loop PI controller parameters were set using the symmetric optimum method.

Proposed control structure is achieved in *dq* reference frame which rotates with grid voltage angular frequency. In order to detect the grid voltage angle, phase locked loop (PLL) is used. *d*-axis of the *dq* reference frame is aligned with the grid voltage vector so the *d*-axis grid voltage is equal to its magnitude ($u_{\mathrm{g}d} = u_{\mathrm{g}}$) while the *q*-axis grid voltage is equal to zero ($u_{\mathrm{g}q} = 0$).

TABLE II
SIMULATION MODEL PARAMETERS

Grid-side inverter	
$V_{\mathrm{ll,\,RMS}}$	400 V
Frequency	50 Hz
Switching frequency	3 kHz
Step-up transformer	
$L_{\mathrm{tr,\,u}}$, $L_{\mathrm{tr,\,v}}$, $L_{\mathrm{tr,\,w}}$	$31,85\,\mu\mathrm{H}$
$R_{\mathrm{tr,\,u}}$, $R_{\mathrm{tr,\,v}}$, $R_{\mathrm{tr,\,w}}$	$1,97\,\mathrm{m\Omega}$
LC filter	
C_{uv} , R_{vw}, R_{uw}	$136\,\mu\mathrm{F}$
L_1 , L_2, L_3	$0,04561\,\mathrm{mH}$
R_1 , R_2, R_3	$0,12\,\mathrm{m\Omega}$
DC link	
C_{DC} (two parallel $5,88\,\mathrm{mF}$ capacitors)	$11,76\,\mathrm{mF}$
R_{p}	$12575\,\Omega$
Braking choppper	
R_{c}	$1,33\,\Omega$
Switch on	$U_{\mathrm{DC}} \geq 800\,\mathrm{V}$
Switch off	$U_{\mathrm{DC}} \leq 775\,\mathrm{V}$
IGBT	
$U_{\mathrm{CE,\,s}}$	1200 V
$U_{\mathrm{C,\,nom}}$	400 A
Generator-side inverter	
$U_{\mathrm{ll,\,RMS}}$	400 V
Frequency	50 Hz
Switching frequency	2 kHz
R_4, R_5, R_6	$0,197\,\mathrm{m\Omega}$
L_4, L_5, L_6	$0,07451\,\mathrm{mH}$

The outer DC voltage control loop keeps the DC voltage at reference value, which ensures that the produced active power is transferred from the DC circuit to the grid. Output of the DC voltage PI controller is the *d*-axis grid current reference. Calculated grid current references are inputs to the PI controllers. In order to achieve decoupled control in the *d*- and the *q*-axes, decoupling signals are added to outputs of PI controllers as follows:

$$\Delta u_{\mathrm{g}d} = u_{\mathrm{g}d} - \omega L_{\mathrm{f}} i_{\mathrm{g}q}, \tag{1}$$

$$\Delta u_{\mathrm{g}q} = u_{\mathrm{g}q} - \omega L_{\mathrm{f}} i_{\mathrm{g}d}. \tag{2}$$

Setting $i^*_{\mathrm{g}q}$ to zero keeps the unity power factor. Real output power is controlled by setting $i^*_{\mathrm{g}d}$. Both output current controller parameters are set according to the symmetric optimum method.

B. Generator-side inverter control

Fig. 4 shows the generator-side inverter control scheme. Switches are the same as for the grid-side inverter, consisting of three bidirectional IGBT-freewheeling diode pairs per phase leg. An SVPWM control scheme is used, enabling control over generator real and reactive power components, as well

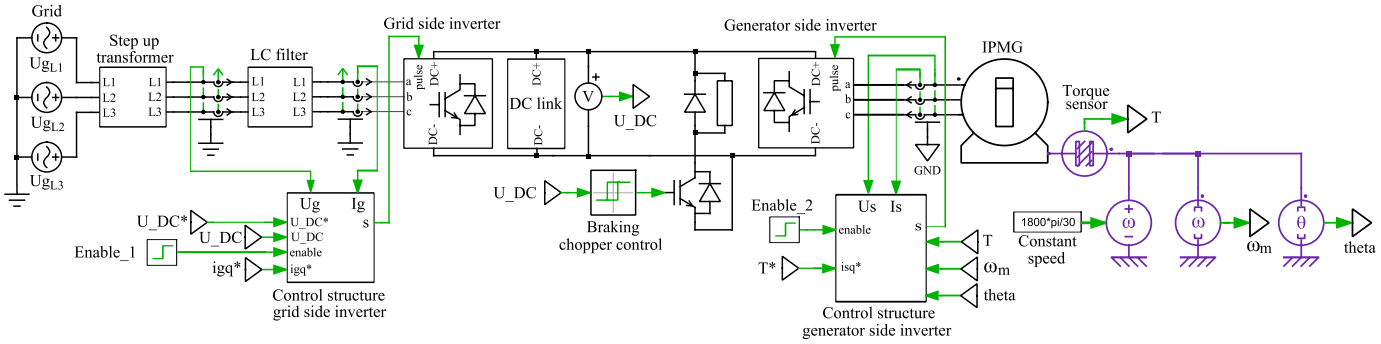

Fig. 2. Converter simulation model

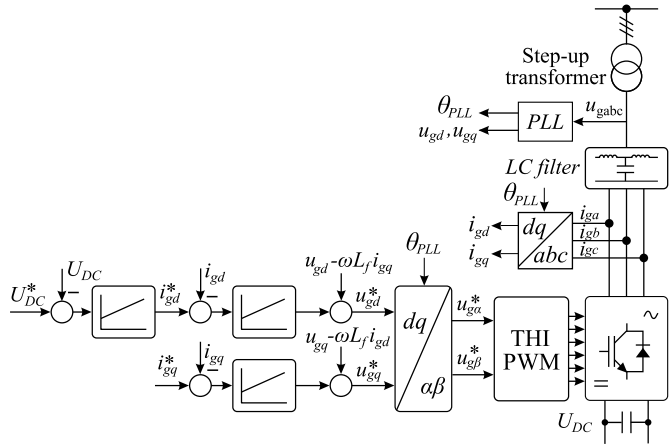

Fig. 3. Grid-side inverter control structure

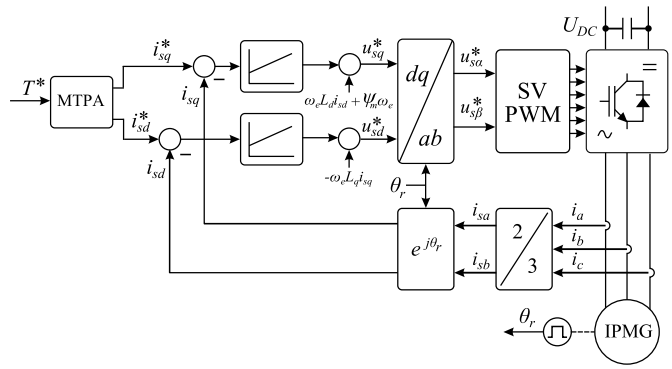

Fig. 4. Generator-side inverter control structure

as control over *d*- and *q*-axis generator stator currents. Such a control scheme is needed to obtain the MTPA algorithm.

Fig. 4 shows that the control structure from Fig. 2 consists of three PI controllers. Reference values for *d* and *q* axis current components, i_{sd}^* and i_{sq}^*, are calculated via MTPA algorithm. MTPA algorithm is a widely spread control method, due to the fact it exploits reluctance torque, achieving the maximum electromagnetic torque per amp.

The algorithm is based on internal permanent magnet synchronous generator (IPMSG) electromagnetic torque equation in *dq* coordinate system. Let p be the number of generator pole pairs, i_{dq} stator current vector in *dq* coordinate system, Ψ_f generator stator flux linkage, L_d i L_q stator inductances in *d*- and *q*-axis, respectively, i_{sd} and i_{sd} stator current components in *d*- and *q*-axis, respectively. Generator electromagnetic torque is given as follows:

$$T_\mathrm{em} = \frac{3}{2} p \left(\Psi_\mathrm{f} i_{dq} + \left(L_d - L_q \right) i_{sd} i_{sq} \right). \tag{3}$$

Let β be the angle between current i_{dq} and *q*-axis of the *dq* coordinate system, in a way that:

$$i_{sq} = |i_{dq}| \cos(\beta), \tag{4}$$

$$i_{sd} = |i_{dq}| \sin(\beta) \tag{5}$$

is valid. Generator electromagnetic torque can be expressed as:

$$T_\mathrm{em} = \frac{3}{2} p \left(\Psi_\mathrm{f} I_\mathrm{s} \cos(\beta) + \left(L_d - L_q \right) I_\mathrm{s}^2 \sin(\beta) \cos(\beta) \right), \tag{6}$$

where I_s is the stator current vector amplitude:

$$I_\mathrm{s} = |i_{dq}| = \sqrt{i_{sd}^2 + i_{sq}^2}. \tag{7}$$

The electromagnetic torque maximum value per amp is calculated by deriving equation (6) with respect to angle β. Final solution is a function of one of two stator current components:

$$\begin{aligned} f_\mathrm{MTPA}(i_{sd}) = i_{sd}^4 + \frac{3\Psi_\mathrm{f}}{L_d - L_q} i_{sd}^3 + \frac{3\Psi_\mathrm{f}^2}{\left(L_d - L_q\right)^2} i_{sd}^2 + \\ + \frac{3\Psi_\mathrm{f}^3}{\left(L_d - L_q\right)^3} i_{dq} - \frac{16 T_\mathrm{em}^2}{9p^2 \left(L_d - L_q\right)^2} = 0, \end{aligned} \tag{8}$$

$$f_\mathrm{MTPA}(i_{sq}) = \left(L_d - L_q\right)^2 i_{sq}^4 + \frac{2T_\mathrm{em}}{3p} \Psi_\mathrm{s} i_{sq} - \left(\frac{2T_\mathrm{em}}{3p} \right)^2. \tag{9}$$

Each of the equations (8) or (9) will, after substituting in (6), give an optimal solution for currents i_{sd} and i_{sq}, such that the stator current vector amplitude I_s is the smallest possible for a given torque value. Both equations, (8) and (9), are of fourth order. A fourth-order polynomial can be solved in several ways. Due to its ease of implementation on a digital system, the Ferrari method was chosen. Polynomial (8) solution, after substituting in (6), is an ordered pair:

$$(i_{sd}, i_{sq}) = \left(-\frac{\mathrm{A}}{4} - \frac{\eta}{2} - \frac{\mu}{2}, \frac{\frac{2T_\mathrm{em}}{3p}}{\Psi_\mathrm{f} + \left(L_d - L_q\right) i_{sd}} \right), \tag{10}$$

where

$$\mathrm{A} = \frac{3\Psi_\mathrm{f}}{L_d - L_q}, \tag{11}$$

$$\mathrm{B} = \frac{3\Psi_\mathrm{f}^2}{\left(L_d - L_q\right)^2}, \tag{12}$$

$$\mathrm{C} = \frac{3\Psi_\mathrm{f}^3}{\left(L_d - L_q\right)^3}, \tag{13}$$

$$d = -\frac{16T_\mathrm{em}^2}{36p^2\left(L_d - L_q\right)^2}, \tag{14}$$

$$\alpha = \frac{1}{3}\left(3\mathrm{AC} - 12d - \mathrm{B}^2\right), \tag{15}$$

$$\beta = \frac{1}{27}\left(-\mathrm{B}^3 + 9\mathrm{ABC} + 72\mathrm{BD} - 27\mathrm{C}^2 - 27\mathrm{A}^2 d\right), \tag{16}$$

$$\gamma = \frac{\mathrm{B}}{3} + \sqrt[3]{-\frac{\beta}{2} + \sqrt{\frac{\beta^2}{4} + \frac{\alpha^3}{27}}} + \sqrt[3]{-\frac{\beta}{2} - \sqrt{\frac{\beta^2}{4} + \frac{\alpha^3}{27}}}, \tag{17}$$

$$\eta = \sqrt{\frac{\mathrm{A}^2}{4} - \mathrm{B} + \gamma}, \tag{18}$$

$$\mu = \sqrt{\frac{3}{4}\mathrm{A}^2 - \eta^2 - 2\mathrm{B} \pm \frac{1}{4\eta}\left(4\mathrm{AB} - 8\mathrm{C} - \mathrm{A}^3\right)}. \tag{19}$$

Currents in *d*- and *q*-axes which give the maximum electromagnetic torque for minimum generator stator current can be determined using this method.

C. Converter loss model

Papers [3]–[5] have shown that converter losses depend on the utilized modulation method.

Power converter losses are determined according to converter loss model in [6]. Converter losses consist of switching and conduction losses. Both losses are dependant on the converter operating point: switching losses on currents at which switchings take place, and conduction losses on conduction currents and saturation voltages. Both values are a part of semiconductor datasheets. Therefore, switching and conduction losses are operating point-dependant, and are found in semiconductor datasheets.

Converter losses are analyzed separately from the rest of the simulation, based on recorded current and voltage waveforms for each inverter phase leg. If both the source and load are symmetrical (both conditions are met, since the source is a symmetrical three-phase generator, and the load is the electrical grid), converter losses are the same for all semiconductor switches within the converter. A single switch consists of an IGBT and an accompanying freewheeling diode.

Converter losses were calculated using an averaged loss model, since they were calculated separately from the rest of the results, based on recorded current and voltage waveforms. An average loss model is based on an assumption that the converter switching frequency is sufficiently larger than the modulation signal frequency, i.e. that the frequency modulation index, m_f, is sufficiently large. In case the frequency index is large enough (its value is at least 40 in this case), current flowing through a switch can be considered constant within a single switching period.

In that case, an approximate method can be used to determine semiconductor losses by fitting the current-dependant, i.e. operating point-dependant, switching and conduction losses datasheet values with a higher-order polynomial (2nd or higher). Switching losses are fitted from semiconductor current-dependant switching energy datasheet values, while conduction losses are fitted from conduction voltage-dependant semiconductor current datasheet values.

Conduction losses can be calculated from semiconductor current-voltage characteristics datasheet values, enabling conduction losses to be written as a function of load current amplitude. These losses can be reduced to those of the fundamental current harmonic, so that the converter conduction losses are:

$$P_\mathrm{cond} = \mathrm{c}I_1 + \mathrm{d}I_1^2, \tag{20}$$

where coefficients c and d are determined by fitting the conduction losses curve, and I_1 is the load current fundamental harmonic RMS value.

Switching losses are calculated from the datasheet switching current-dependant switching energy curves (switch-on and switch-off energy curves). If a large enough frequency modulation index is assumed, a switch switches on and off at the same current value, so that both switch-on and switch-off energies are calculated for the same current value. Since both energies are calculated for the same current value, switch-on and switch-off energies can be added to form a total switching energy curve for one switching period. Dividing the total switching energy with the load current fundamental harmonic, function $k(I_1)$ is obtained:

$$k\left(I_1\right) = \frac{E_\mathrm{sw,\,tot}}{I_1} = \mathrm{a} + \mathrm{b}I_1 + \mathrm{c}I_1^2. \tag{21}$$

Coefficients a, b and c are calculated by fitting the datasheet values with a 2nd order polynomial. Total switching losses of a single switch are:

$$P_\mathrm{sw,\,tot} = E_\mathrm{sw,\,tot} f_\mathrm{s} = \left(\mathrm{a} + \mathrm{b}I_1 + \mathrm{c}I_1^2\right) I_1 f_\mathrm{sw}. \tag{22}$$

Switching frequency is a constant, known in advance as one of preset values. Generator-side inverter switching frequency is set to 2 kHz, and grid-side inverter switching frequency is set to 3 kHz.

D. LC filter loss model

LC filter design is explained in detail in [7]–[9], and its stability analysis in [10]. *LC* filter loss model is based on the *LC* filter equivalent circuit, modelled as a parallel-series connection of a capacitor and an inductor, per phase. Capacitor equivalent series resistances (ESR) are several orders of magnutide smaller than capacitor leakage resistances and inductor ESRs. Accordingly, capacitor losses modelled via ESRs were neglected. Since capacitor leakage resistances are several orders of magnitudes larger than inductor ESRs, leakage resistances were also neglected. Therefore, *LC* filter losses were modelled via inductance ESRs.

Inductor losses consist of copper and core losses. Since core losses of an inductor are, to some extent, operating

point-independant, copper losses sufficiently large at nominal operating point to disregard core losses were assumed. Hence, *LC* filter losses were modelled as inductor copper losses.

This way, *LC* filter losses were simulated via measured ouput currents and inductor winding resistances from Table II.

E. Step-up transformer loss model

Step-up transformer losses were modelled as copper winding losses, for the same reason as for the *LC* filter. Transformer losses were determined from the transformer model, based on measured winding currents.

F. DC link loss model

DC link capacitors were selected based on [11]. DC link losses were modelled via ESR and leakage resistor. Since ESR is several orders of magnitude smaller than the leakage resistance, and the fact that only the DC link voltage is measured (a common practice in industrial enviroments), DC link losses were modelled using leakage resistance. DC link consists of two capacitors, hence DC link losses are modelled with two parallel-connected resistances R_{p}.

III. Results

This section compares simulation results presented in Section II. Results are compared for a change in converter power, ranging from 0 kW to 520 kW. Simulation results from Section III-A show that a change in DC link voltage does not influence converter losses.

Generator and grid converter losses, along with *LC* filter and DC link losses, are analyzed via the developed simulation model. Current THD factors for the generator and grid-sides at converter connection points are also analyzed. A change in generator real power, spanning from idle to nominal power, was completely analyzed at nominal working conditions. Influence a change in grid voltage amplitude, a change in DC link voltage and a change in DC link capacitor capacitance have on the converter losses and efficiency, as well as on the aforementioned THD factors was also analyzed.

A. Simulation results at nominal operating point

The first simulation simulates energy transfer from the wind turbine generator ($50\,\mathrm{Hz}$, $\cos(\varphi) = 1$) to the electrical grid (50 Hz). The DC link voltage is set to 650 V, while the reference value of the converter q-axis current is set to zero, in an effort to keep unity power factor of the grid-side inverter. Fig. 5 shows the converter losses and voltage and current THDs for a change in generator real power, spanning from 0 kW to 520 kW. Table II contains the simulation parameters. Simulations are firstly done for a set of parameters which represent the targeted nominal operating point of the converter.

Fig. 5 clearly shows an increase in switching and conduction losses caused by an increase in converter power. *LC* filter and DC link losses have little effect on converter efficiency, which exceeds 98%, which is in accordance with realistic expectations for converters of similar power ratings. Current

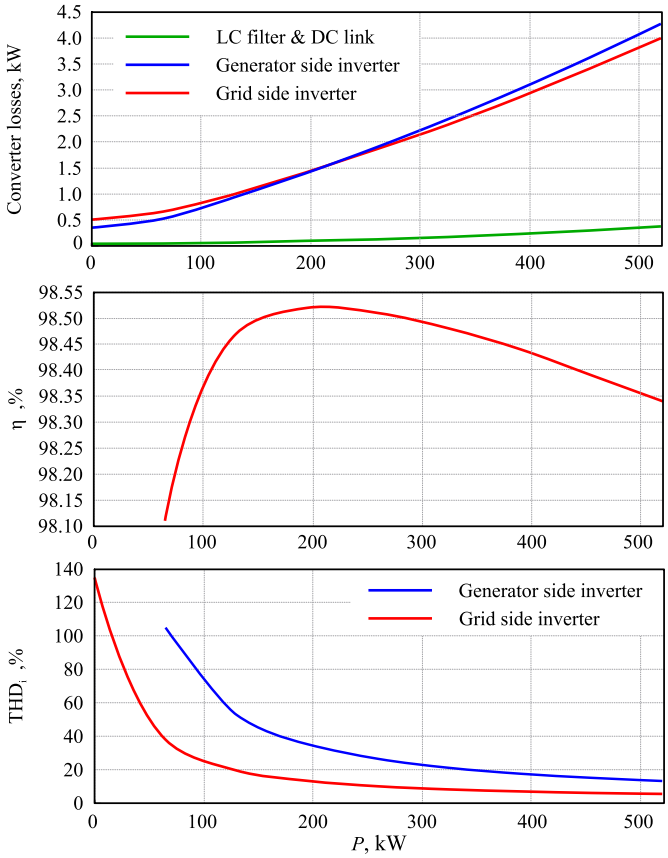

Fig. 5. Converter losses, voltage and current THD at nominal operating point

THD decreases with increasing converter power and is around 5% for nominal operating point.

B. Simulation results for various operating points

Operating points were varied, including changes in grid voltage (ranging from 0.9 per unit to 1.1 p.u.) changes in DC link voltage (ranging from 650 V to 750 V) and changes in reference power (ranging from zero to 500 kW).

Fig. 6 shows the DC link voltage and converter power reference. An increase in converter power increases the DC link voltage ripple. Voltage ripple at nominal operating point changes within $\pm 0,46\%$ for a set voltage of 650 V.

The results show grid-side inverter losses, generator-side losses, *LC* filter and DC link losses and output voltage and current THD, for different generator real power, ranging from idle to nominal generator power. Apart from the nominal operating point, the aforementioned results are shown for a change in grid voltage amplitude, a change in DC link voltage and a change in DC link capacitor capacitance. These results have shown that when the converter power is increased, THD is decreased, due to an increase in the fundamental current harmonic amplitude. On the other hand, converter power loss increases, lowering the energy conversion efficiency. Maximum efficiency operating point was determined. Fig. 1 shows an example of the obtained results for the nominal operating

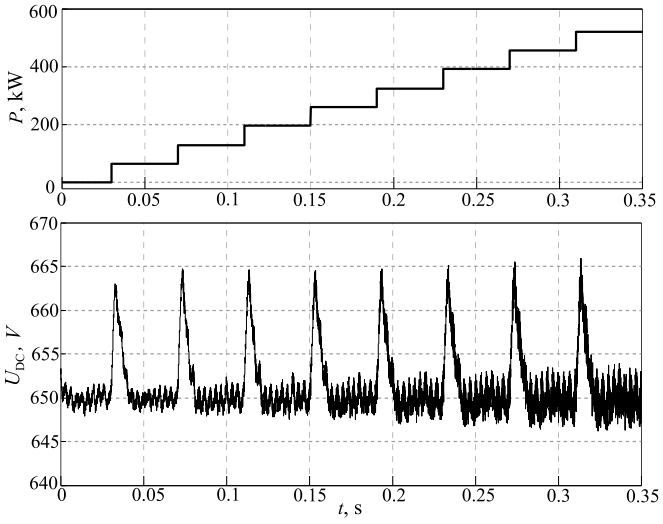

Fig. 6. DC link voltage and generator-side power reference

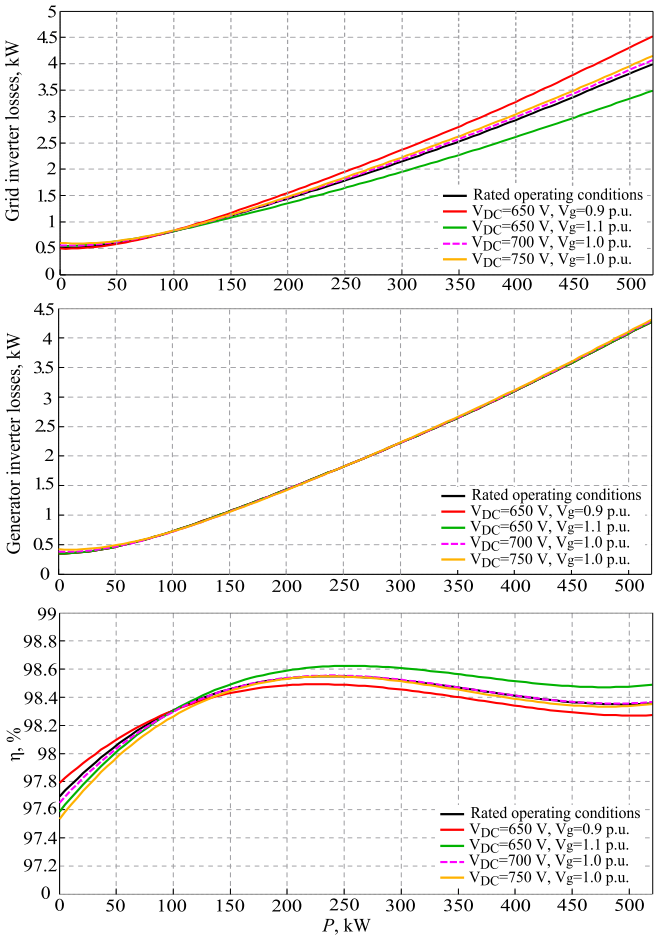

Fig. 7. Generator and grid converter losses and overall converter efficiency for various operating conditions

point: grid- and generator-side inverter losses, converter efficiency and grid- and generator-side current THD.

Fig. 7 shows a comparison between grid-side inverter losses,

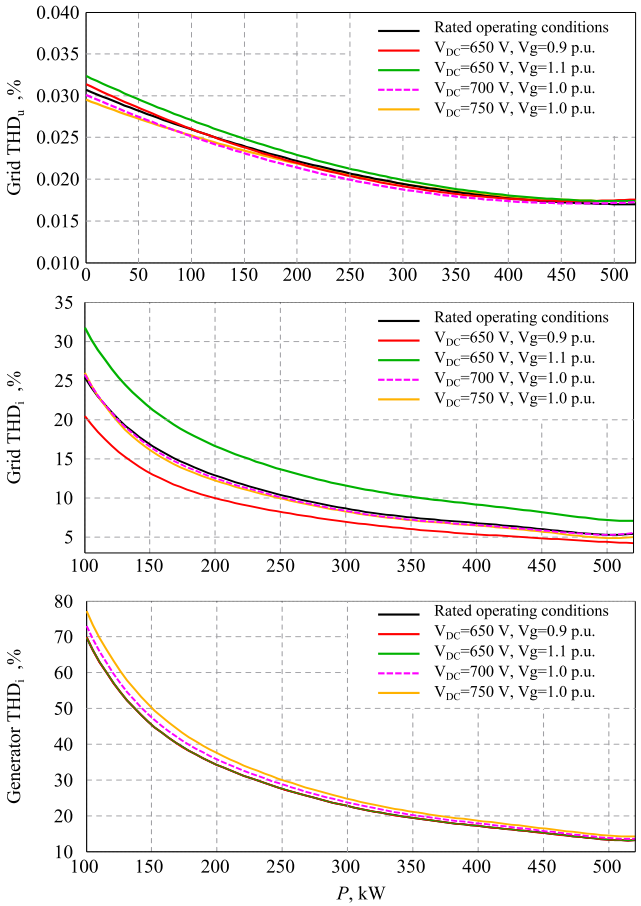

Fig. 8. Grid voltage and current THD, and generator current THD for various operating conditions

generator-side inverter losses and converter efficiency for various operating conditions.

A grid voltage drop below nominal value causes the largest converter losses. The reason behid this phenomenon is an increase in output current needed to keep the power constant. Lowest grid converter losses occur for nominal DC link voltage and increased grid voltage by 10%.

Difference between converter losses for different simulated operating conditions is barely noticeable. This means that the total converter losses are lowest for an increase in grid voltage.

Largest converter efficiency occurs for an increase in grid voltage, as was concluded earlier. As expected, converter efficiency decreases for a decrease in grid voltage, due to an increase in converter output current.

Fig. 8 shows grid voltage THDs, as well as grid and generator current THDs. Voltage THDs are low for all simulated operating conditions, not exceeding 0,035%. Fig. 8 shows that voltage THDs are the same on both ends of the converter.

Unlike converter losses, output current THD is the lowest for a decrease in grid voltage, which is caused by an increase in output current. Simulation results show that an increase in output current causes a decrease in current THD.

A change in DC link or grid voltage have no significant

effect on figures of merit of energy quality of the converter generator-side.

Analysis showed that the nominal operating conditions are optimal. Simulation results showed that a change in either grid or DC link voltage does not have a significant effect on generator-side voltage and current THDs. The aforementioned voltage changes do not effect the generator-side inverter losses. A decrease in grid voltage increases grid-side inverter losses, due to an increase in converter output current. Simultaneously, an increase in output current decreases output current THD.

IV. Conclusion

A two-level back-to-back power converter simulation model was presented, used for connecting an internal permanent magnet generator to the electrical grid. Structure of the whole system was explained in detail, as well as generator- and grid-side inverter control structures. A basic review of the used grid-side inverter control structure was given, as well as a more detailed description of the method used to determine the MTPA algorithm parameters, used for generator-side inverter control. A method to determine the converter, *LC* filter and step-up transformer losses, as a system contributing to energy transfer from generator to the electrial grid, was described. Simulation results showing total converter losses, grid- and generator-side inverter losses, overall converter efficiency, grid voltage THD and converter voltage and current THDs were given. DC link voltage step responses for different converter power references were simulated, ranging from zero to nominal converter power. Converter losses and THD simulation results were given for nominal operating point and changes in DC link and grid voltages. Results show that the *LC* filter and step-up transformer losses have little influence on overall energy transfer system losses. Grid current THD value drops with an increase in converter power, due to a linear increase in fundamental output current harmonic, and a significantly lesser increase in carrier and sideband current harmonics amplitudes. On the other hand, a larger power reference causes larger converter losses, due to the increase in fundamental output current harmonic amplitude. The largest decrease in converter efficiency is caused by a decrease in grid voltage amplitude, due to a significant increase in fundamental converter output current harmonic, caused by a fairly small impedance connecting the converter and step-up transformer. Largest converter efficiency was achieved for DC link nominal voltage, and electrical grid voltage amplitude of 1,1 pu, due to a decrease in fundamental output current harmonic. Conversely, such voltage distribution causes an increase in grid current THD. Results show that grid voltage changes have no effect on generator-side inverter losses, nor current THD.

Future research will include experimentally measured grid-side and generator-side inverter losses, whose results will be compared to results obtained by simulations.

Acknowledgment

This work has been fully supported by the Croatian Science Foundation under the project number UIP-2013-11-7601.

References

[1] V. Yaramasu, B. Wu, P. C. Sen, S. Kouro, and M. Narimani, "High-power wind energy conversion systems: State-of-the-art and emerging technologies," *Proceedings of the IEEE*, vol. 103, no. 5, pp. 740–788, 2015.

[2] G. C. Konstantopoulos and A. T. Alexandridis, "Full-scale modeling, control, and analysis of grid-connected wind turbine induction generators with back-to-back ac/dc/ac converters," *Emerging and Selected Topics in Power Electronics, IEEE Journal of*, vol. 2, no. 4, pp. 739–748, 2014.

[3] N. Holtsmark and M. Molinas, "Loss comparison of matrix and back-to-back converters for offshore wecs," in *Transmission and Distribution Conference and Exposition (T&D), 2012 IEEE PES*, pp. 1–6, IEEE, 2012.

[4] D. Hou, C. Hu, G. Li, and F. Zhu, "Analysis of frequency inverter loss under 3 different pwm modulation methods," in *Modelling, Identification & Control (ICMIC), 2014 Proceedings of the 6th International Conference on*, pp. 18–21, IEEE, 2014.

[5] M. C. Cavalcanti, E. R. Da Silva, D. Boroyevich, W. Dong, and C. B. Jacobina, "A feasible loss model for igbt in soft-switching inverters," in *Power Electronics Specialist Conference, 2003. PESC'03. 2003 IEEE 34th Annual*, vol. 4, pp. 1845–1850, IEEE, 2003.

[6] U. Drofenik and J. W. Kolar, "A general scheme for calculating switching-and conduction-losses of power semiconductors in numerical circuit simulations of power electronic systems," in *Proceedings of the 2005 International Power Electronics Conference (IPEC'05), Niigata, Japan, April*, pp. 4–8, 2005.

[7] R. Beres, X. Wang, F. Blaabjerg, M. Liserre, and C. Bak, "A review of passive power filters for three-phase grid connected voltage-source converters," 2016.

[8] G. E. Mejia Ruiz, N. Munoz, and J. B. Cano, "Modeling, analysis and design procedure of lcl filter for grid connected converters," in *Power Electronics and Power Quality Applications (PEPQA), 2015 IEEE Workshop on*, pp. 1–6, IEEE, 2015.

[9] K. H. Ahmed, S. J. Finney, and B. W. Williams, "Passive filter design for three-phase inverter interfacing in distributed generation," in *Compatibility in Power Electronics, 2007. CPE'07*, pp. 1–9, IEEE, 2007.

[10] R. Pena-Alzola, M. Liserre, F. Blaabjerg, R. Sebastián, J. Dannehl, and F. W. Fuchs, "Analysis of the passive damping losses in lcl-filter-based grid converters," *Power Electronics, IEEE Transactions on*, vol. 28, no. 6, pp. 2642–2646, 2013.

[11] A. J. Roscoe, S. J. Finney, and G. M. Burt, "Tradeoffs between ac power quality and dc bus ripple for 3-phase 3-wire inverter-connected devices within microgrids," *Power Electronics, IEEE Transactions on*, vol. 26, no. 3, pp. 674–688, 2011.